Techno-economic heat transfer optimization of large scale latent heat energy storage systems in solar thermal power plants

Stefan Hübner[1], Markus Eck[2], Christoph Stiller[3] and Markus Seitz[4]

[1] Dipl.-Ing., Project Engineer, Linde AG, Seitnerstraße 70, 82049 Pullach, Germany, stefan.huebner@linde.com

[2] Dr.-Ing, Professor, University for Applied Science, Albrechtstraße 30, 49076 Osnabrück, Germany

[3] Dr. Ing., Project Manager, Linde AG, Seitnerstraße 70, 82049 Pullach, Germany

[4] Dipl.-Ing., Project Engineer, German Aerospace Center (DLR), Institute of Engineering Thermodynamics, Pfaffenwaldring 38-40, 70569 Stuttgart, Germany

Abstract

Concentrated solar power plants with integrated storage systems are key technologies for sustainable energy supply systems and reduced anthropogenic CO_2-emissions. Developing technologies include direct steam generation in parabolic trough systems, which offer benefits due to higher steam temperatures and, thus, higher electrical efficiencies. However, no large scale energy storage technology is available yet. A promising option is a combined system consisting of a state-of-the art sensible molten salt storage system and a high temperature latent heat thermal energy storage system (LHTESS).

This paper discusses the systematic development and optimization of heat transfer structures in LHTESS from a technological and economic point of view. Two evaluation parameters are developed in order to minimize the specific investment costs. First, the specific product costs determine the optimum equipment of the latent heat storage module, i.e. the finned tube. The second parameter reflects the interacting behavior of the LHTESS and the steam turbine during discharge. This behavior is described with a simplified power block model that couples both components.

Keywords

Latent heat storage, phase change material, heat transfer enhancement, direct steam generation

Nomenclature

Specific product costs	C_{product}	€/kWh$_{\mathrm{th}}$
Specific levelized costs of electricity	$C_{\mathrm{LCOE,LHTESS}}$	€/MWh$_{\mathrm{el}}$
Specific operation & maintenance costs	$C_{\mathrm{O\&M}}$	€/a
Inner tube diameter	d_{i}	mm
Energy	E	J
Latent heat factor	f	–
Specific mass enthalpy	h_{v}	J/kg
Investment costs	I	€
Length	l	m
Mass flow	$\dot{m}, m_{\mathrm{dot}}$	kg/s

Annual storage cycle	n_{cycle}	#/a
Heat flux density	$\dot{q}$	W/m²
Pressure	p	bar
Discount rate	r	%
Temperature	T	°C
Temperature difference	ΔT	K
Time	t	sec, a
Depreciation time	t_{dep}	a
Tube pitch	t_p	m
Heat transfer coefficient	α_{PCM}	W/m²/K

CSP	Concentrated solar power	NL	Nominal load
DNI	Direct normal irradiance	O&M	Operation and maintenance
DSG	Direct steam generation	PL	Part load
FEM	Finite element method	PCM	Phase-change-material
HTF	Heat transfer fluid	SF	Solar field
LCOE	Levelized cost of electricity	SoC	State of charge of LHTESS
LHTESS	Latent heat thermal energy storage system	TES	Thermal energy storage

1 Introduction

1.1 DSG solar power plants

State-of-the-art concentrated solar power (CSP) plants use thermal oil as heat transfer fluid (HTF). This limits the maximum operation temperature to 400°C and, thus, the overall plant efficiency. Instead, solar thermal power plants based on direct steam generation (DSG) with steam temperatures up to 550°C offer higher efficiencies [1,2]. For further cost reduction cost efficient thermal energy storage (TES) system is required. However, a latent heat storage system that absorbs and provides the heat of evaporation is not commercially available.

This paper focuses on the design optimization of the latent heat storage system's main equipment, i.e. vertical tubes equipped with fins. Longitudinal fins manufactured by extrusion allow very flexible and adaptable fin design and low manufacturing costs. In addition, longitudinal fins lead to minimum mechanical load on the fins, when the phase change material (PCM) volume changes due to the solid-liquid phase change.

The considered latent heat storage system is a part of a combined latent-sensible TES system as proposed by Seitz et. al. [3]. The design basis is a CSP plant with a nominal power output of 50 MW_{el}, a solar field capacity of 250 MW_{th} with a solar multiple of 2 and a direct normal irradiation of 850 W/m² (e.g. Andasol plant). The maximum discharge time of the fully charged storage system is set to 8 hours. Sodium nitrate with a phase change temperature of

306°C is applied as latent heat storage medium, while the solar salt, a mixture of 60 % sodium nitrate and 40 % potassium nitrate, is used as the sensible storage medium.

1.2 Heat transfer enhancement in latent heat storage systems

In high temperature latent heat storage systems alkali salts such as sodium nitrate or potassium nitrate are typically used [3]. However, these materials have a very low thermal conductivity in the range of 0.5 W/m/K. However during freezing heat transfer is constraint by thermal conduction, since natural convection at the solid-liquid borderline is severely limited. According to Pointner et.al, [4], there are different concepts of how to overcome the limited heat transfer rate. On the one hand stationary systems with either an increased effective thermal conductivity or an extended heat transfer area have been researched. On the other hand the overall heat transfer rate can be improved by moving the PCM and avoiding the constantly growing solid layer.

Stationary systems

Steinmann and Tamme, [5], and Do Couto Aktay et al., [6], have investigated enhancing the thermal conductivity by integrating the PCM into a matrix of highly conductive material such as expanded graphite. Although they applied different manufacturing techniques, experimental results showed different disadvantages such as anisotropic thermal conductivity and dynamic material parameters due to thermal cycling.

In contrast, the concept of applying fins to the heat transfer fluid (HTF) tubes was studied successfully in different small and mid-scale experiments. Bayón et al. [7] demonstrated the evaporation and condensation of water/steam in a 100 kW_{th} test facility by using graphite foil fins. Another 200 kW_{th} graphite fin based storage module was integrated into a sand-lime bricks plant for waste heat recuperation purposes [8]. In order to avoid reactions between graphite and nitrate salts, which occur at temperatures exceeding 250°C, aluminum fins have been introduced [9]. Based on the results of a lab module a 700 kWh_{th} demo plant using radial aluminum fins in $NaNO_3$ was developed and built. The system was successfully operated in fixed and sliding pressure mode simulating its combination with a DSG solar power plant [10, 11]. A further improvement was achieved due to the application of longitudinal fins that are clipped to the steel tube with a special steel clip. This clip concept enables the assembly to cope with different thermal expansion factors and is suitable for mass production. It was successfully operated for approximately 200 cycles in a lab scale plant consisting of seven tubes [12].

An alternative method is to macro-encapsulate the PCM in tubes or spheres enabling direct heat transfer between the HTF and the encapsulated PCM. These spheres have been investigated widely in low temperature applications [13]. However, in high temperature applications using alkali salts as PCM only steel and nickel with an internal polymer coating have been identified as a noncorrosive and temperature resistive encasing material [14]. Tamme et al. [15] and Buschle [16] reported that in comparison to an external PCM arrangement this technique is less efficient due to a higher amount of required encasing material.

2 Methods and Calculations

The optimization of the LHTESS's heat transfer structure is based on a finite-element method (FEM) simulation model being applied to a multitude of heat transfer structures. The set up and boundary conditions of this model are being explained in chapter 2.1, whereas chapter 2.2 presents the three main targets and the general optimization procedure. This includes the development and the parameterization of different heat transfer structures and fin profiles as well as an overview of all compared structures. The main evaluation parameter – the specific product costs – that is calculated from the FEM simulation results is introduced in chapter 2.3. A second parameter – the levelized cost of electricity (LCOE) is then introduced in chapter 2.4, in order to prove the validity of the main evaluation parameter. Finally chapter 2.5 presents the model for coupling the power block and the LHTESS that is required for calculating the LCOE parameter.

2.1 Numerical simulation Model

In order to optimize the LHTESS's heat transfer structures it is assumed that all tubes and fin profiles are identical and that HTF distribution is uniform across all tubes. At discharge the storage system is operated in forced circulation mode with high volume flows. Thus, freezing along the length of the tubes takes place simultaneously as it has been observed in 3-D simulations. As a consequence, only a two-dimensional cross section of one finned tube is considered for simulation. The cross section consists of a central steel tube with 25.4 mm in outer diameter, the extruded fin profile of variable size and the surrounding PCM. The extruded fins cohere to a second central tube of the same material that is mounted on the inner steel tube. Both central tubes have a wall thickness of 2 mm. The whole structure is enclosed by the basic geometry, i.e. a hexagon, a square or a triangle, that holds the phase change material (Figure 1). Only these three basic geometries allow for a dense packing of multiple tubes inside the LHTESS without any additional void volume between the tubes. Finally, the size of the basic geometry determines the tube pitch.

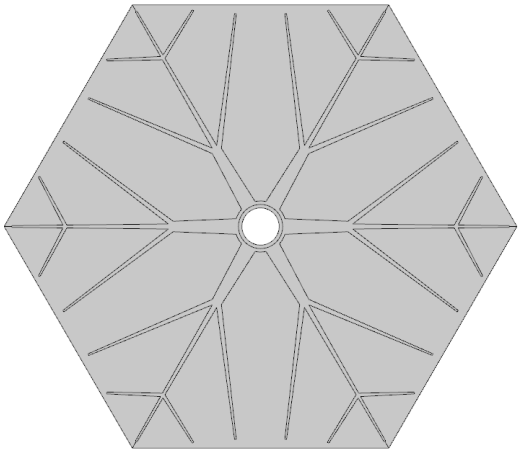

Figure 1: Fin profile inside the basic hexagonal geometry with 2nd order fin branching level

The freezing process with a growing resistive solid layer on the heat transfer surface is considered to be the limiting process that dictates the LHTESS's design. At discharge the cold HTF enters the tubes from the bottom limiting the occurrence of natural convection to a minimum. Hence, the heat transfer problem is reduced to a transient heat conduction problem that is solved with Comsol Multiphysics®. The software applies a finite element method and the phase change problem is addressed by the apparent heat capacity formulation.

Prior to the FEM-simulation a detailed verification of the simulation model has been performed based on the analytical solution of a simple 1-D semi-infinite case [17]. Adequate results at acceptable computation times were obtained for a free triangular mesh with "finer" sized elements and the intermediate time stepping method with a maximum time step of 2 seconds. A further reduction of computation time is achieved by taking advantage of symmetries within each fin profile. Thus, only a sixth or a quarter of each profile of Figure 1 has to be simulated.

The evaporation of water inside the steel tube is described by a Neumann boundary condition. A typical heat transfer coefficient of evaporating steam is 10,000 W/m²/K and the constant temperature is the evaporation temperature. The outside of the basic geometry is connected to identical basic geometries of surrounding tubes. Thus, an adiabatic boundary condition is applied here. Furthermore, typical material parameters of carbon steel and an aluminum alloy (series 6000) are applied to the tube and fins. The material properties of the chosen PCM are taken from [18] and the starting and boundary conditions are listed in Table 1.

Table 1: Main FEM-simulation Parameter

NaNO3					
Solid density	kg/m³	2113	Liquid density	kg/m³	1908
Solid heat capacity	J/kg/K	1655	Liquid heat capacity	J/kg/K	1655
Solid thermal conductivity	W/m/K	0.6	Liquid thermal conductivity	W/m/K	0.51
Latent heat	kJ/kg	178	Melting temperature T_{melt}	°C	306
Boundary conditions					
Heat transfer coefficient α_{evap}	W/m²/K	10,000	Evaporation temperature T_{evap}	°C	296
Starting temperature T_{start} (t = 0)	°C	307	Temperature difference ΔT_{LHTESS} ($T_{melt} - T_{evap}$)	K	10
Tube length l_{tube}	m	15	Inner tube diameter d_i	mm	21.4

2.2 Optimization procedure of heat transfer structures

The study pursues three main objectives. The first one is to determine the optimum basic geometry. Due to cost efficiency reasons, a large scale storage module should aim at lowest inactive PCM volume between tubes and fins. Considering the 2-D cross section, there are only three basic geometries that allow a perfect packing without inactive volume, i.e. triangles, squares and hexagons.

The study's second target is to identify the optimum heat transfer structure in one basic geometry. Simple heat transfer structures are single tubes without fins or a simple star-shaped fin profile with the number of main fins according to the number of corners of the basic geometry. In contrast to the "star" profiles, complex fin profiles with multiple fins and fin branches up to third order branches are being developed and investigated.

Thirdly, the study compares whether it is beneficial to apply steel fins or aluminum fins. On the one hand steel fins could provide a significant potential to reduce manufacturing cost by avoiding the bi-metal connection with different thermal expansion factors. On the other hand aluminum fins have high thermal expansion factors and are less expensive with regard to the material volume.

The study examines numerous heat transfer structures that are clustered in fin profile classes. These classes are named according to the following structure. In 6A2.1 the first number indicates the basic geometry's number of edges and the letter 'A' describes the general trapezoid fin shape. The classes are then distinguished according to their chronological development as expressed with the second figure. Finally, the last figure indicates a slight variation of the main class, for example by applying a different fin material. A classification of all developed and considered fin profile classes is shown in Table 2. Images of all profile classes can be found in the supplementary data section.

Within each fin profile class the optimum geometry size and the optimum fin shape have to be identified. The geometry size is changed based on the tube pitch parameter, whereas the variation of fin length, thicknesses and rotation angles specifies the fin shape. This class optimization allows for an efficient comparison of each fin class' optimum, in order to determine the most efficient heat transfer structure.

The main boundary conditions of fin design are a maximum and minimum fin thickness of 9 and 1 mm, respectively due to manufacturing constraints. Further, the number of main fins being connected to the central tube varies between 4 to 12 and 4 to 8 fins for hexagon and square geometries, respectively.

Table 2: Classification and quantity of examined fin profile classes

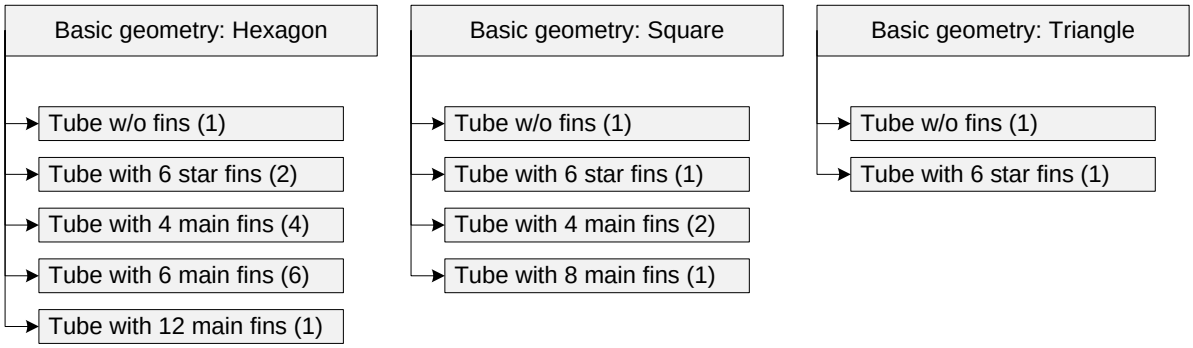

2.3 Calculation of specific product costs

In order to compare the heat transfer structures the specific product cost is introduced as the main evaluation parameter. The specific product cost $C_{product}$ (eq. 1) is defined as the sum of the specific cost of material C_{material} and manufacturing $C_{\text{manufacturing}}$ of a steel tube equipped with a certain fin profile divided by its energy output E_{out} after 8 hours of discharge (eq. 2). The energy output is based on the fin profile's integrated heat flux $\dot{q}_{fin}$ multiplied with the heat transfer surface (eq. 3). In this equation the required tube length is set to 15 m and the heat flux is obtained from the numerical simulation. The material cost include the material cost of steel, aluminum and the PCM itself, whereas manufacturing costs take into account the extrusion of the fin profile and its mounting on the steel tubes based on the clip solution by [12]. Finally, welding cost for the connection of each single tube to the upper and lower distributor system are added to the manufacturing cost. This cost parameter indicates whether it is worthwhile to increase the size of the fin profile or not. Large fin sizes lead to larger basic geometries reducing the overall amount of tubes. In contrast, the required amount of fin material grows above average if longer distances of heat conduction have to be incorporated. All considered specific material and manufacturing costs are listed in Table 3. Further costs such as the storage vessel itself and costs of peripheral devices like distribution system, steam drums etc. are not included, due to their independency of the fin profile and tube number.

$$C_{\text{product}} = \frac{\sum C_{\text{material}} + \sum C_{\text{manufacturing}}}{E_{\text{out}}} \qquad \text{(eq. 1)}$$

$$E_{\text{out}} = d_{\text{i}} \cdot l_{\text{tube}} \cdot \int_{t=0}^{t=8\,h} \dot{q}_{\text{fin}} \qquad \text{(eq. 2)}$$

Table 3: Cost parameter

Product cost					
Steel tubes	€/kg	3	Aluminum material	€/kg	2
Fin profile extrusion per half-shell	€/kg	2 – 3	Connection of tubes and fin profile	€/m	7.5 – 12.5
Welding costs	€/tube	100 – 150	PCM costs	€/kg	1

Solar field cost					
Spec. solar field invest	€/m²	200	Effective DNI	W/m²	850
Collector efficiency	%	65	Solar field size for TES charge	MW_{th}	125
Latent heat share f_{latent}	%	65	O&M costs	%	2.5
Discount rate r	%	8	Storage cycle n_{cycle}	#/a	150
Depreciation time t_{dep}	a	20			

2.4 Levelized cost of electricity (LCOE)

The specific product cost (chapter 2.3) is calculated based on a constant temperature difference ΔT_{LHTESS} and a constant water mass flow. However, when coupling the LHTESS and the steam turbine the system is operated with a constantly increasing temperature difference and a constantly reducing mass flow over SoC (see section 2.5). As a consequence, the parameters that descend from the specific heat transfer structure impact the electricity generation and thus the techno-economic performance of the overall system significantly. This impact is investigated by introducing an additional evaluation parameter, i.e. the LHTESS's levelized cost of electricity $C_{\mathrm{LCOE,LHTESS}}$. However, as the study's target is to compare heat transfer structures of the LHTESS, the parameter states the LCOE of the LHTESS, only. It does not include the required sensible storage system for pre- and superheating.

The $C_{\mathrm{LCOE,LHTESS}}$ values are calculated by dividing the system's investment and operation and maintenance (O&M) costs C_{storage} by the annually generated electrical energy E_{turbine}. The investment includes the already listed material and manufacturing costs of the finned tubes, the solar field investment for charging the storage system as well as the LHTESS's and solar field's O&M costs. Both, solar field investment and O&M costs are related to the latent heat storage part only as mentioned above. The latent heat share of the overall amount of stored heat depends on the operating pressure and the life steam temperature. For the values chosen in this study it is in the range of 65 % and thus, being incorporated into the calculation as a factor f_{latent}. Similarly, the generated electric energy has to be multiplied with the latent heat factor (eq. 5 – 7). The calculation procedure of E_{turbine} is explained in detail in chapter 2.5. All assumptions made for calculating the specific LCOE are listed in Table 3.

$$C_{\mathrm{LCOE,LHTESS}} = \frac{C_{\mathrm{storage}}}{E_{\mathrm{turbine}}} \quad \text{(eq. 3)}$$

$$C_{\mathrm{storage}} = I_{\mathrm{SF}} \cdot f_{\mathrm{latent}} + \sum C_{\mathrm{material}} + \sum C_{\mathrm{manufacturing}} + \sum_{t=0}^{t=t_{\mathrm{dep}}} \frac{C_{\mathrm{O\&M}} \cdot f_{\mathrm{latent}}}{(1+r)^t} \quad \text{(eq. 4)}$$

$$E_{\mathrm{turbine}} = \sum_{t=0}^{t=t_{\mathrm{dep}}} \frac{E_{\mathrm{el}} \cdot f_{\mathrm{latent}} \cdot n_{\mathrm{cycle}}}{(1+r)^t} \quad \text{(eq. 5)}$$

2.5 Part load operation of LHTESS coupled with the steam turbine

If the LHTESS is coupled with the steam turbine there are two possible part load operation modes that take into account the LHTESS's decreasing thermal power during discharging. In fixed pressure mode the water mass flow is adjusted by maintaining a constant water pressure and thus, a constant temperature difference $\Delta T_{\mathrm{LHTESS}}$ between evaporation temperature of water and PCM's phase change temperature. In sliding pressure mode the water mass flow is kept constant and the temperature difference $\Delta T_{\mathrm{LHTESS}}$ is increased by lowering the water pressure. Laing et al. [11] have shown that the LHTESS itself can be operated in both modes, but that the sliding pressure mode is the preferred one in combination with the steam turbine. However, a direct coupling of LHTESS's and steam turbine's part load behavior has not been reported previously. Thus, a simple power block model is developed, describing the combined operation.

The model consists of two main calculation parts, one for the LHTESS and one for the steam turbine. Both parts are iterated until the evaporated water mass flow inside the LTHESS $\dot{m}_{\mathrm{H2O}}$ equals the steam turbine's inlet mass flow $\dot{m}_{\mathrm{PL}}$.

First, the LHTESS's thermal power $\dot{Q}_{\mathrm{LHTESS}}$ and the evaporated mass flow $\dot{m}_{\mathrm{H2O}}$ are calculated according to (eq. 3). This calculation requires an assumption of the temperature difference $\Delta T_{\mathrm{LHTESS}}$ that defines the evaporation pressure p_{evap}, the specific fin profile's heat transfer surface A_{HEX} per meter tube length and the maximum energy content per meter of one 2-D fin profile cross section (Figure 1). The heat transfer coefficient α_{PCM} is obtained from each fin profile's specific heat flux $\dot{q}_{\mathrm{fin}}$ related to the inner tube surface per meter tube length. It describes the overall heat transfer from the steel tube through the fins into the PCM. As a result the declining evaporation pressure for different steam mass flows over LHTESS's state of charge can be observed on the left side of Figure 2 (No. 1).

$$\dot{Q}_{\mathrm{LHTESS}}(SoC) = \alpha_{\mathrm{PCM}}(SoC) \cdot A_{\mathrm{hex}} \cdot \Delta T_{\mathrm{LHTESS}} = \dot{m}_{\mathrm{H2O}}(SoC) \cdot (h_{\mathrm{v}}'' - h_{\mathrm{v}}') \quad \text{(eq. 6)}$$

If pressure drops inside the heat exchangers for superheating are neglected, the LHTESS's evaporation pressure is equivalent to the turbine's live steam pressure $p_{\mathrm{in,PL}}$ (see Figure 2, No. 2). Based on that assumption the steam turbine's part load steam mass flow $\dot{m}_{\mathrm{PL}}$ can be calculated according to Stodola's law given in eq. 4 [19].

$$\frac{\dot{m}_{\mathrm{PL}}}{\dot{m}_{\mathrm{NL}}} = \sqrt{\frac{p_{\mathrm{in,PL}}^2 - p_{\mathrm{out,PL}}^2}{p_{\mathrm{in,NL}}^2 - p_{\mathrm{out,NL}}^2} \cdot \frac{T_{\mathrm{in,NL}}}{T_{\mathrm{in,PL}}}} \quad \text{(eq. 7)}$$

This equation includes the steam turbine's inlet and outlet pressures both in nominal and part load, the live steam temperature and the steam mass flow, both in part load and nominal load operation. The nominal load operation parameters are given by steam turbine design during daytime operation, the part load live steam temperature is assumed to be at maximum discharge temperature of 520°C. The iterative calculation of eq. 3 and 4 has to be executed

until both steam mass flows are equivalent (Figure 2, No. 3). Then the generated electric power results from expanding the steam mass flow in the steam turbine.
Solving this iterative calculation stepwise for all SoCs, a detailed LHTESS and steam turbine part load operation curve is obtained. Here, the SoC level at which the discharge is stopped is set to 5 %. At this SoC the simulation results show a significant decrease in discharge power, because discharged heat is only supplied by subcooling the PCM. This simplified model involves the following assumptions and simplifications.

- No pressure drop in LHTESS and superheating section
- No impact on boiler feed water temperature and thus, the preheating section → only full evaporation without preheating and superheating is taking place in the LHTESS
- Sufficient energy and temperature for steam superheating is available → constant live steam temperature of 520°C
- No steam turbine limitation due to steam wetness → no mass flow for reheating required and thus, total steam mass flow is expanded from live steam pressure till condenser pressure
- Constant condenser pressure of 100 mbar
- Adiabatic part load efficiency of steam turbine according to part load operation mode is included

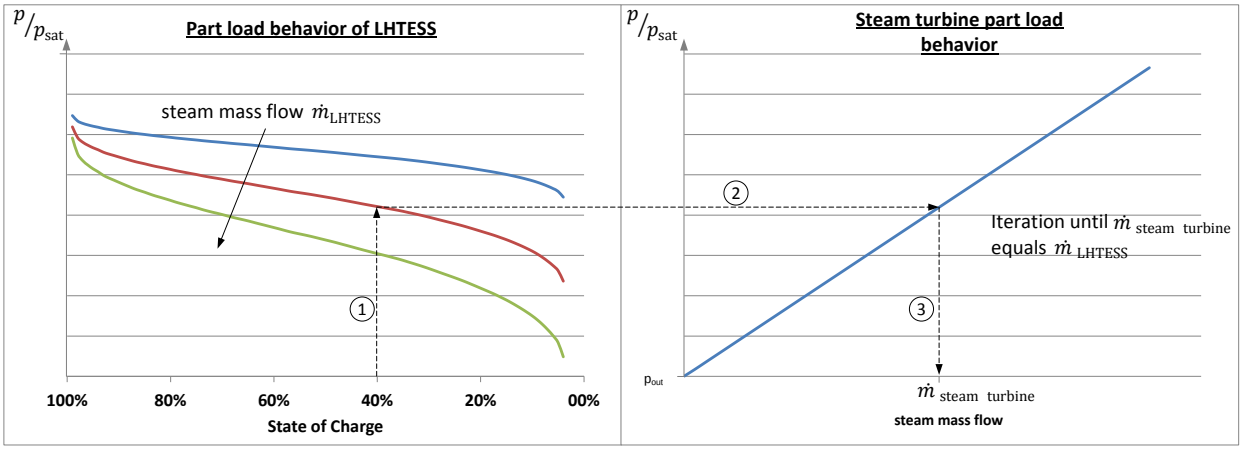

Figure 2: Model set up of connected LHTESS and steam turbine

3 Results and discussion

3.1 Profile optimization based on specific product costs

The determination of each profile classes' minimum product costs is shown exemplarily for class 6A4.2. All simulations clearly show lowest specific product costs for a simultaneous freezing of the PCM within the considered basic geometry. The PCM in each compartment between two adjacent fins should freeze with the same speed as it does in all other compartments. In a perfect profile the last liquid droplets of all compartments freeze at the same time. Thus, all fin surfaces provide a certain heat flux during the whole discharge time. If one or more single fins are idle for a certain time due to a fully frozen compartment, the whole fin profile is oversized leading to higher specific product costs. A simultaneous freezing process is depicted in in Figure 3 showing the uniform temperature distribution in each of the compartments at different time steps.

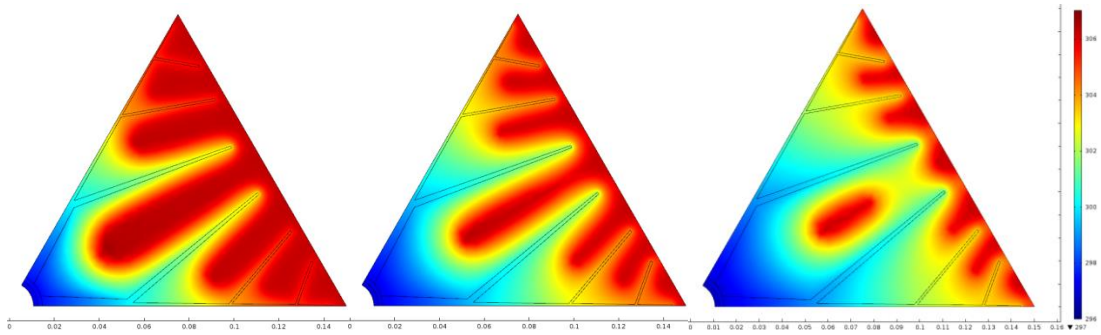

Figure 3: Freezing process of Geo-6A4.2 with t_p = 260 mm at 4 h, 6 h and 6.45 h

Once the fins are determined according to their optimum position, specific length and angle, one can optimize the size of the basic geometry. In this optimization the tube pitch parameter that determines the size of the basic geometry is the only independent parameter, because the fin lengths are correlated to its size. The optimum tube pitch, i.e. lowest specific product costs occur when the available PCM energy is completely discharged exactly within the specific time of 8 hours. This is due to the fact that PCM's cost fraction is in the range of 45 to 50 % of overall specific product costs. If the basic geometry becomes smaller, the share of aluminum to aluminum plus PCM volume per meter increases. On the one hand this leads to higher discharge powers and thus, discharge is completed in less than 8 hours. On the other hand the aluminum material and manufacturing costs increase and so do the specific product costs. The fin profile is oversized. The other way around, larger basic geometries lead to undersized fin profiles because the share of aluminum to aluminum plus PCM volume per meter decreases. The product costs rise again due to lower discharge powers and an energy utilization factor below 100% within 8 hours. In this study the optimum share of aluminum to PCM volume per meter for an 8 hour discharge cycle is found to be 9.5 %.

These results differ slightly when tubes without a fin profile or with simple star-fin profiles are being evaluated. Lower overall heat fluxes lead to smaller optimum tube pitches, which in turn leads to higher amount of tubes. This increases the specific welding costs significantly

and thus, reduces the PCM cost share. Now, specific product costs are lowest, when only ~ 80 to 90 % of the maximum available energy is discharged.

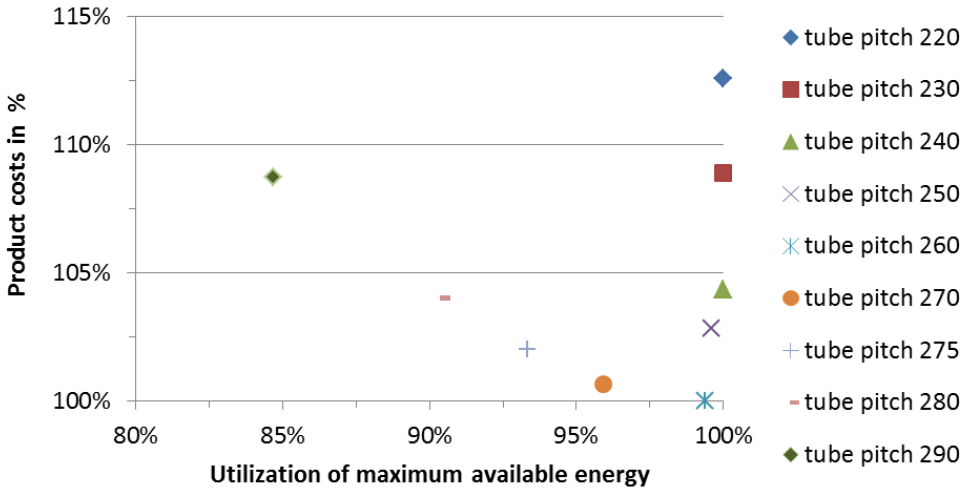

Figure 4: Specific product costs optimization of Geo-6A4.2

3.2 PCM storage system coupled with steam turbine

LHTESS and steam turbine's part load behavior

During part load operation the steam turbine characteristics allows for a robust control of the LHTESS operation. In the beginning of the discharge process the LHTESS's heat transfer coefficient α_{PCM} is very high. In order to maintain a constant turbine inlet volume flow, the steam turbine characteristics result in a high steam pressure. This in turn, results in a low temperature difference $\Delta T_{\mathrm{LHTESS}}$ in the storage system, limiting the overall heat and steam mass flow. In contrast, at low SoCs with small heat transfer coefficients and volume flows a low steam turbine inlet pressure occurs and hence, the temperature difference in the LHTESS increases. Now, the mass flow to be evaporated increases and mitigates the decline of power output. In other words, declining heat transfer in the LHTESS is compensated by the turbine's suction behavior.

The slowly declining evaporation pressure and the increasing temperature difference during discharging are depicted in Figure 5. The power output curves of the LHTESS and steam turbine correlate with the evaporation pressure. Further, Figure 5 shows that the turbine power decreases only by 17 % percentage points; i.e. from 89 % at full SoC to 72 % at 5 % SoC. These power output curves are in line with the curves obtained by a detailed power block model simulated in Ebsilon®Professional.

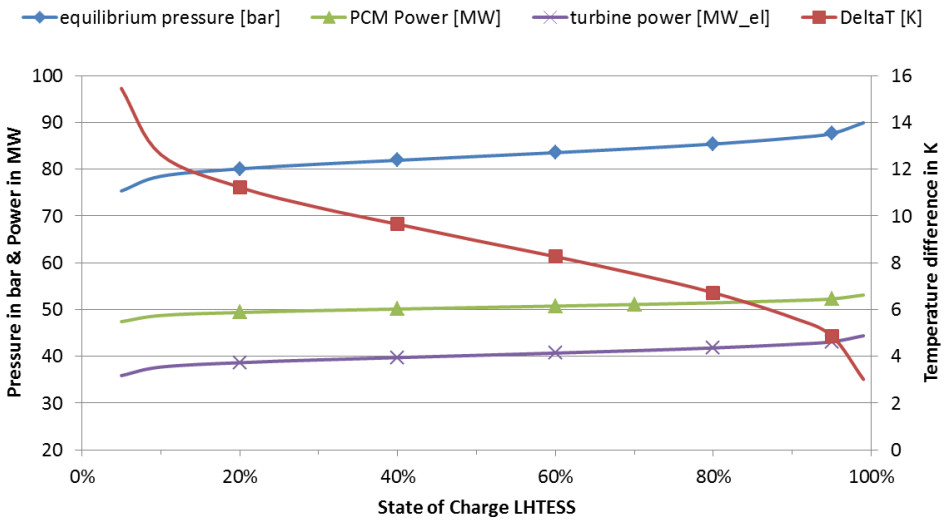

Figure 5: Specific part load behavior of LHTESS with Geo-6A4.2_260 and steam turbine

LHTESS size optimization

According to the part load behavior we can determine the real discharge time of the latent heat storage system and its optimum size in MWh_{th}. As described above the steam turbine always levels the LHTESS's power and thus, the power output cannot exceed or fall below that certain range. Thus, the real discharge time only depends on the size of the storage system. An oversized storage system with a high storage capacity cannot be completely discharged within 8 hours. Being undersized in terms of storage capacity it will be completely discharged in less than 8 hours.

Based on the nominal turbine power of 50 MW_{el}, the real discharge time and the specific LCOE are calculated for different nominal storage capacities showing minimum costs at a storage capacity of 425 MWh_{th}. This size corresponds very well to the real discharge time of 8 hours (Figure 6).

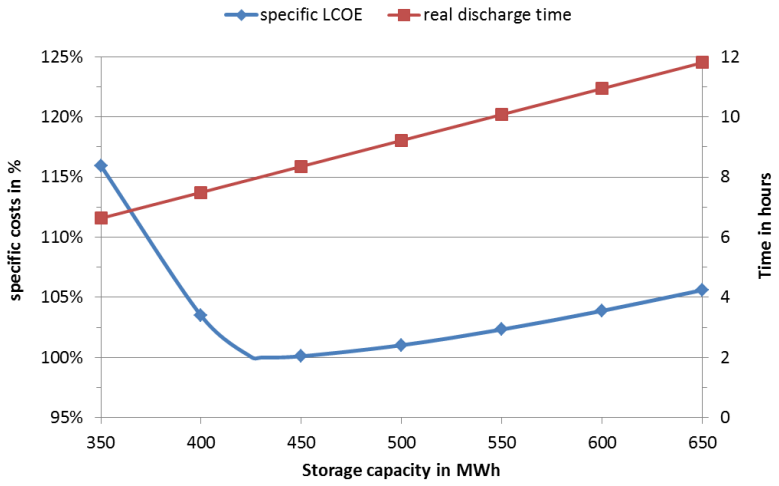

Figure 6: Latent heat storage capacity optimization

Profile optimization based on LCOE

Comparing the specific LCOE for different fin profiles a similar cost structure as in Figure 4 is observed. Again, the minimum costs of complex fin profiles are obtained for profiles that enable a full use of available PCM heat However, the LCOE are less sensitive to the manufacturing and material costs of the LHTESS. According to eq. 6 the overall investment costs include the solar field costs that account for up to 70 %. Due to the higher costs, optimum complex fin profiles tend to be slightly oversized, i.e. optimum tube pitch is about 5 to 10 mm smaller than in case of product cost optimization. These smaller basic geometries assure a complete utilization of available PCM energy. In case of geometry 6A4.2 the lowest LCOE are obtained for a 255 mm tube pitch, whereas the optimum tube pitch according to specific product costs was 260 mm. Nevertheless, the difference in LCOE is less than 1 % signifying that specific product cost parameter is sufficient for a detailed profile evaluation.

Considering non-ideal "no-fin" and "star-fin" profiles the lowest LCOE occur for slightly undersized profiles. However these profiles are less undersized than according to the product cost optimization. The optima are found for a utilization of PCM energy between 90 and 98 %.

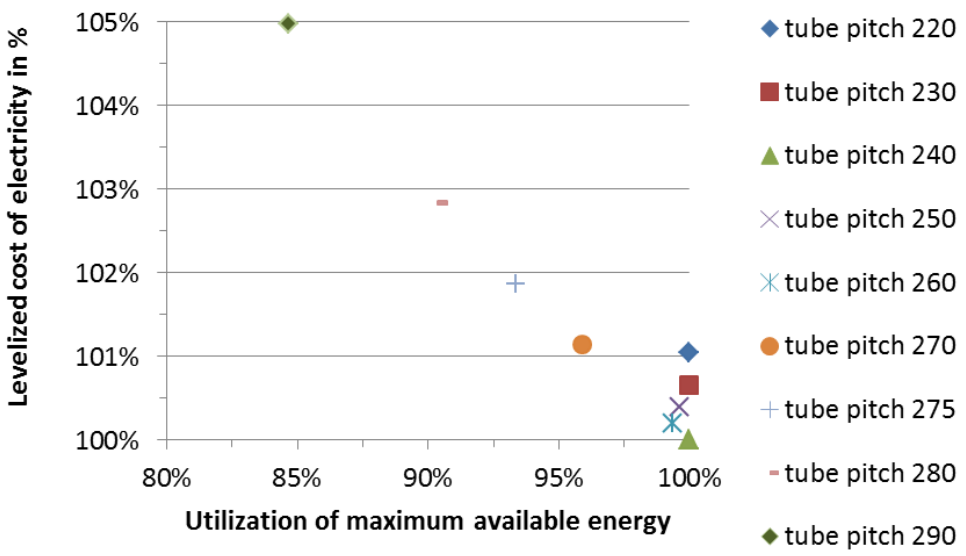

Figure 7: Specific LCOE costs optimization of Geo-6A4.2

3.3 Further design rules

Basic geometries

The comparison of PCM freezing in basic geometries has been executed for a tube without fins, and for tubes equipped with a simple star fin profile. It is shown that in both cases hexagon geometries provide lowest specific product costs. "No-fin" tubes in square and triangle basic geometries lead to 5 % and 13 % higher product costs respectively as shown in column one to three in Figure 8. For "star-fin" tubes the specific product costs of square and

triangle basic geometries are about 12 to 15 % higher (column four to six in Figure 8). Neither by optimizing complex fin profiles in squares can the minimum product costs of similar profiles in hexagons be reached. Thus, we conclude that cost-wise hexagons are the basic geometry of choice, which is due to their highest similarity to the ideal circle geometry.

Fin profile optimization

Simple "star-fin" profiles in hexagon geometries already provide 20 % and 6 % lower specific product and LCOE costs when compared to "no-fin" profiles. Considering the optimum fin profile in a hexagonal basic geometry presented in column 8, these costs can even be reduced to 66 % and 86 % of "no-fin" profile's product and LCOE costs, respectively. The optimum size of this fin class 6A4.2 is 260 mm. With this dimension and 15 m tube length about 5,200 tubes are required for a 425 MWh_{th} storage system. The overall welding costs contribute about 4.4 % to the overall specific product costs. This cost share increases to 10 % for "star-fin" profiles and to 44 % for the "no-fin" profile. The absolute amount of welding costs of "no-fin" and "star-fin" profiles exceeds Geo-6A4.2's welding costs by a factor of 14, i.e. ~ 73,000 tubes, and by a factor of about 2, i.e. 12,000 tubes, respectively. However, the sum of the remaining investment costs of all three profiles is in the same range. Thus, the main advantage of finned tubes is given by the significant reduction of required tubes and its welding costs to the distributor system. In addition, fin material and extrusion costs contribute about 35 to 40 % to the overall product costs. Both costs types depend on the specific weight of the fin profile, indicating that a detailed fin optimization is necessary and worthwhile.

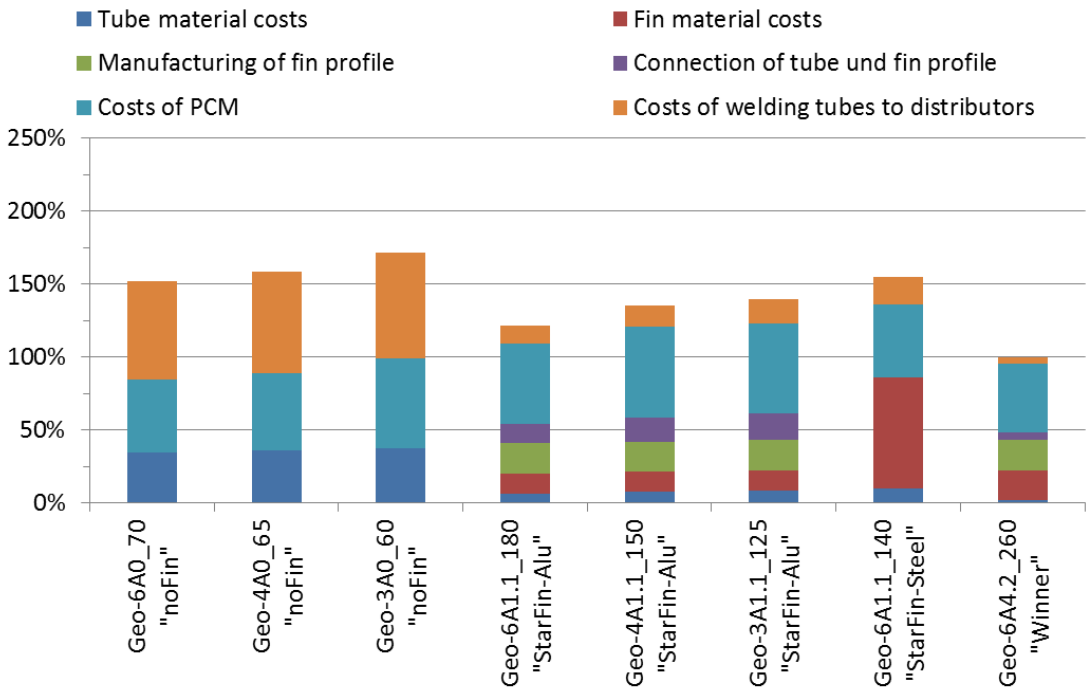

Figure 8: Comparison of optimum fin profiles of different fin profile classes

The comparison of "star-fin" profiles with extruded aluminum fins and steel fins made of simple steel sheets in a hexagon basic geometry is shown in Figure 8. Steel fins compared to aluminum fins provide a lower thermal conductivity, but could offer significant manufacturing cost reduction. In the most optimistic case neither manufacturing costs for the steel fins nor costs for connecting steel tube and steel fins are considered. However, even in this scenario it is observed that steel-fin tubes are not a competitive option for LHTESS from a cost point of view. These tubes have 28 % higher specific product costs than the same profile made of aluminum fins. The fin material costs increase by a factor of 5 compared to aluminum fins, contributing about 49 % to the overall product costs. As a consequence of lower discharge powers and smaller tube pitches, the number of tubes required and thus, the welding costs increase significantly.

Number of main fins and fin branching

The comparison of many different fin profile classes showed that there is an optimum amount of main fins that are connected to the central tube. In hexagon geometries different fin profile classes with four, six and twelve main fins have been developed and optimized. The results clearly show that fin profiles with six main fins result in lowest specific product and LCOE costs. Applying four main fins, there is too little fin material in the center of the geometry in order to transport the heat from the central tube to the outside areas of the hexagon geometry. Applying twelve main fins, the central part around the tube is almost completely filled with aluminum leading to an over-supply of heat/cold in this zone. The over-supply leads to partially frozen (sub-) compartments after shorter time-periods resulting in inefficiency as explained in chapter 3.1.

In addition, the results show that due to the limited maximum and minimum fin thickness a third fin branching level leads to inefficiencies. At each branching the overall heat flux is split up according to the number of new fins. Thus, fin thickness should be adapted accordingly.

4 Conclusions

The paper introduces a methodology for a techno-economic optimization of heat transfer structures in large scale latent heat energy storage systems and its results. Two evaluation parameters have been developed, the specific product costs and the LCOE of the LHTESS not considering the sensible storage part. The first parameter C_{product} considers the product costs for tubes, fins, manufacturing of finned tubes and the costs of the PCM itself. These costs are related to the available energy in the storage system at constant discharge conditions. The LHTESS's levelized costs of electricity C_{LCOE} take into account all product and investment costs as well as O&M costs related to the generated electrical energy. In order to calculate the electrical energy, a simplified model coupling the part load behavior of LHTESS and the steam turbine of a concentrated solar power plant is set up and used. In general, both evaluation parameters are in very good agreement, when being applied to different heat transfer structures with and without fins.

First of all, the study shows that hexagons are the basic geometry of choice. Although squares and triangles as well allow for a perfect packing of single tubes without inactive PCM volume in between, hexagons provide lowest specific product and LCOE costs.
Second, comparing simple star fin profiles made of aluminum and steel fins a clear benefit of aluminum as fin material is observed. On the on hand steel fins could provide much lower manufacturing costs, but on the other hand the fin material costs increase significantly in combination with lower discharge powers.
Finally the overall comparison of optimized heat transfer structures clearly demonstrates the cost reduction potential of tubes equipped with complex aluminum fin profiles. The product costs' main cost driver is the number of finned tubes that is required for a certain storage capacity. Complex fin profiles require about 2 to 14 times less tubes compared to simple "star-fin" profiles or a "no-fin" profiles. This proves that the detailed profile optimization according to the application scenario provides significant potential for further cost reduction of LHTESS.

Acknowledgements

The authors thank the German Federal Ministry of Economic Affairs and Energy for the financial support given to the DSG-Store project (Contract No. 0325333A and 0325333D).

Nomenclature

References

[1] Feldhoff JF, Schmitz K, Eck M, Schnatbaum-Laumann L, Laing D, Ortiz-Vives F, Schulte-Fischedick J; Comparative system analysis of direct steam generation and synthetic oil parabolic trough power plants with integrated thermal storage; Int J Solar Energy 2012 vol 86 pp. 520 – 530

[2] Feldhoff JF, Benitez D, Eck M, Riffelmann KJ; Economic potential of solar thermal power plants with direct steam generation compared with HTF plants; J Solar Energy Engineering 2010 vol 132, 041001–9.

[3] Seitz M., Cetin P., Eck M.; Thermal storage concept for solar thermal power plants with direct steam generation; Energy Procedia No. 49 (2014) pp. 993 – 1002

[4] Pointner H, Steinmann WD, Eck M; "Introduction of the PCM Flux concept for latent heat storage"; Energy Procedia 2014 vol 57 pp. 643 – 652

[5] Steinmann WD, Tamme R; "Latent heat storage for solar steam systems"; J Solar Energy Engineering 2007 vol 130, 011004

[6] Do Couto Aktay KS, Tamme R, Mueller-Steinhagen H; "Thermal Conductivity of High-Temperature Multicomponent Materials with Phase Change"; Int J Thermophysics 2008 vol 29 pp. 678 – 692

[7] Bayón R. Rojas E, Valenzuela L, Zarza E, León J; "Analysis of the experimental behavior of a 100 kW_{th} latent heat storage system for direct steam generation in solar thermal power plants"; Int J Applied Thermal Engineering 2010 vol 30 pp. 2643 – 2651

[8] Lovegrove K, Stein W; “Concentrating Solar Power Technology – Principles, Developments and Applications”; Woodhead Publishing 2012 ISBN: 978-1-84569-769-3

[9] Laing D, Bauer T, Steinmann WD, Lehmann D; Advanced high temperature latent heat storage systems – design and test results; 11th Int Conference on Thermal Energy Storage – Effstock 14-17 June 2009 in Stockholm, Sweden

[10] Laing D, Bahl C, Bauer T, Lehmann D, Steinmann WD; Thermal energy storage for direct steam generation; Int J Solar Energy 2011 vol 85 pp. 627 – 633

[11] Laing D, Eck M, Hempel M, Steinmann WD, Meyer-Gruenefeldt M, Eickhoff M; „Analysis of operation test results of a high temperature phase change storage for parabolic trough power plants with direct steam generation”; Proceedings of the ASME 2012 6th Int conference on Energy Sustainability

[12] Laing D, Bauer T, Breidenbach N, Hachmann B, Johnson M; “Development of high temperature phase-change-material storages”; Int J of Applied Energy 2013 vol 109 pp. 497 – 504

[13] Sharma SD, Sagara K; “Latent Heat Storage Materials and Systems: A Review”; Int J of Green Energy 2005 vol 2 pp. 1 – 56

[14] Bellan S, Gonzalez-Aguilar J, Romero M, Rahman MM, Goswami DY, Stefanakos EK; “Numerical investigation of PCM- based thermal energy storage system”; Int J of Energy Procedia 2015 vol 69 pp. 758 – 768

[15] Tamme R, Bauer T, Buschle J, Laing D, Müller-Steinhagen H, Steinmann WD; “Latent heat storage above 120°C for applications in the industrial process heat sector and solar power generation”; Int J of Energy Research 2008 vol 32 pp. 264 – 271

[16] Buschle J, Steinmann WD, Tamme R; “Latent Heat Storage for Process Heat Applications” 10th Int Conf on Thermal Energy Storage 2006

[17] Alexiades V; Mathematical Modeling of Melting and Freezing Processes; Taylor & Francis Washington DC 1992

[18] Bauer T, Laing D, Tamme R; “Characterization of Sodium Nitrate as Phase Change Material”; Int J Thermophysics 2012 vol 33 pp. 91 – 104

[19] Stodola A; ”Steam and gas turbines: with a supplement on the prospects of the thermal prime mover”; McGraw-Hill book company, inc, 1927 – authorized translation from the sixth German edition by Louis C. Loewenstein